

# Improved Particle Swarm Optimization for Rayleigh Wave Frequency-Velocity Spectrum Inversion

Haitao YAN<sup>a, 1</sup>, Zhao LE<sup>a, 1</sup>, Xueming SHI<sup>b, 2</sup>, Hanbing AI<sup>b</sup>, Wei ZHANG<sup>c</sup>,  
Yonglong YANG<sup>a</sup>, Hui YE<sup>a</sup>, Wentao JIN<sup>c</sup>

<sup>a</sup>CCCC Second Highway Consultants Co., Ltd., Wuhan, Hubei, China

<sup>b</sup>School of Geophysics and Geomatics, China University of Geosciences,  
Wuhan, Hubei, China

<sup>c</sup>Wuhan Geo-Detection Technology Co., Ltd., Wuhan, Hubei, China

**Abstract.** Rayleigh wave inversion plays a role in near-surface exploration at high resolution. Conventional dispersion curve inversion methods require to extract the dispersion curves manually, and their success depends heavily on personal experience. Mode misidentification is easily occurred in frequency-velocity spectrum with complex geological conditions, which increases the difficulties to extract the accurate dispersion curve. Full waveform inversion (FWI) is a prospective approach to resolve complex stratigraphic inversions avoiding manual dispersion curve extraction. However, the current application of FWI is limited by several factors, such as cycle-skipping issues, seismic source estimation, dependence on the initial model. Frequency-velocity spectrum inversion (FVSI) is another potential approach for solving complex near-surface problems. The objective function of FVSI is the residual of frequency-velocity spectrum, which makes it unnecessary to extract the dispersion curve manually. In this paper, we present an improved particle swarm optimization (IPSO) for Rayleigh wave FVSI. Compared with traditional particle swarm optimization (PSO), we reduce the swarm size in the later iterations, which enhances the inversion efficiency; we replace the invalid particles with valid ones, which improves the global search capability. The application of both synthetic and field data has achieved good results, demonstrating the applicability and practicability of the IPSO method.

**Keywords.** Rayleigh wave; improved particle swarm optimization; frequency-velocity spectrum inversion; stochastic evolution; invalid particle eliminating

## 1. Introduction

Rayleigh wave exploration is considered to be an efficient method for reconstructing the near-subsurface at high resolution. The multichannel analysis of surface waves (MASW) method [1] is currently the most widely used Rayleigh wave exploration method. The MASW needs to obtain the dispersion curve manually and invert the S-wave velocity profiles by the extracted dispersion curve [2]. The extraction of dispersion curve depends

---

<sup>1</sup> Co-first authors: Haitao Yan and Zhao Le are contributed equally to this study

<sup>2</sup> Corresponding author: Xueming Shi, E-mail: xmshi666@163.com

highly on subjective judgement and personal experience. Energy mixing and pseudo multi-mode are easily occurred in the spectrum with complex geological conditions, making it difficult to manually extract accurate dispersion curves [3]. Additionally, since the calculation of theoretical dispersion curves is based on the assumption of one-dimensional layered model [4, 5, 6], dispersion curve inversion can only solve the problem of horizontal (or near-horizontal) layered medium, which is often not the case in real strata.

Full waveform inversion (FWI) is an attractive geophysical exploration method of inverting the earth model by directly fitting the waveform [7]. FWI does not need to extract the dispersion curve manually and has no restriction on the media distribution, thus, it is considered a promising application and has rapidly developed in recent years [8, 9, 10]. However, FWI is a multi-parameter, multi-extremal and multi-modal problem, and the inversion is always non-linear and non-unique, which is presently limited in field data application [11]. FWI is currently challenged by several elements, such as a high dependence on the initial model, the cycle-skipping problem, and the difficulty of estimating the seismic source in field data. Many studies have been conducted on these issues [12, 13, 14], but the application of FWI in field data is still challenging at present.

Frequency-velocity spectrum inversion (FVSI) is a method of constructing the earth model via fitting the frequency-velocity spectrum (FVS) directly [15, 16, 17, 18]. We convert the waveform to FVS via phase-shift transform [19] in this paper, which enlarges the details of the dispersion compared to the frequency-wavenumber spectrum [20]. Compared with MASW, the FVS contains richer Rayleigh wave propagation information, and there's no need to extract the dispersion curve manually [21], thus, the inversion result of FVSI is more accurate and objective than that of MASW. Compared with FWI, the objective function of FVSI is less bumpy [22], and the relationship between FVS and S-wave velocity is more quasilinear than that between waveform and S-wave velocity [23].

The strategies used for FVSI can be divided into gradient-based local optimal algorithms and stochastic evolution-based global optimal algorithms. In general, local optimization is efficient but highly dependent on the initial model, and global optimization is inefficient but less dependent on the initial model. Particle swarm optimization (PSO), a typical stochastic evolution-based global optimal algorithm [24, 25], has been successfully used in FVSI. In this paper, we propose an improved particle swarm optimization (IPSO) for FVSI based on the study of Le (2024) [26]. In IPSO, we set a large swarm size in the early iterations, which gives the algorithm a wide search space; we reduce the swarm size in the later iterations, which enhances the inversion efficiency. The particles are gradually concentrated in the later iterations, and we refer the particles with close parameters but larger misfits as invalid particles, because they have litter effect on the inversion result. We find the invalid particles and replace them with the same number of randomly generated valid particles. Compared with traditional PSO, IPSO has less computation, higher efficiency, and better capability of searching for globally optimal solutions. We obtain good results in both synthetic and field data inversion through the proposed IPSO strategy, which suggests that it is an effective and practicable tool for retrieving the subsurface structure.

## 2. Methodologies

Since the FVSI via PSO strategy has been described in detail by Le (2024) [26], we briefly introduce it in this paper. The main process of FVSI in this paper can be summarized as follows:

(1) Initial model generation.

The gradient-based local optimal inverse strategies always require a fixed initial model, and their inversion results vary depending on the initial model settings, which always lead to inversion failure when the initial model settings are unreasonable. However, the PSO (or IPSO) algorithm has no need to manually set up the initial model, but generates it randomly within a given range.

(2) Objective function calculation.

Getting the waveform of the trial model via the finite-difference method [27, 28]; changing waveform to FVS through phase-shift transform [19]; the objective function (or misfit) is the root-mean-square error (RMSE) of the theoretical and observed FVS.

(3) Iterative model updating.

Updating the trial model iteratively until the objective function is sufficiently small or the iteration number reaches the maximum.

### 2.1 PSO method

PSO is a typical stochastic evolutionary algorithm inspired by the behavior of a flock of birds searching for food [24]. Each iteration of the PSO algorithm contains several hundred models, the individual model is called a particle, and all the particles called a swarm. We judge the merit of the particles by their objective functions, a particle with a small objective function will have a higher probability of participating in evolution.

The objective function of FVSI is the  $l_2$ -norm of the observed and predicted FVS (Eqs. (1) and (2)).

$$\Phi = \sum \|S_{pre} - S_{obs}\|_2^2 \tag{1}$$

$$S = |\Psi(u)| \tag{2}$$

where  $\Phi$  denotes the objective function;  $S$  is the FVS;  $S^{pre}$  and  $S^{obs}$  are the predicted and observed FVS, respectively;  $u$  represents the time-domain waveform; The symbol  $\Psi$  denotes the phase-shift transform; the symbols  $\| \cdot \|_2$  and  $| \cdot |$  denote the  $l_2$ -norm and modulus of a vector, respectively.

Since other parameters are less important in Rayleigh wave inversion [1], we only invert the S-wave velocity and layer thickness. For instance, a 4-horizontal-layered model has 7 variables (4 velocities and 3 thicknesses). The PSO method does not need to manually set the initial model, which will be randomly and automatically generated by Eqs. (3) and (4).

$$V_s^i = V_s^{\min} + r(V_s^{\max} - V_s^{\min}) \tag{3}$$

$$Thk^i = Thk^{\min} + r(Thk^{\max} - Thk^{\min}) \tag{4}$$

where  $V_s^i$  and  $Thk^i$  are the S-velocity and layer thickness of the  $i^{th}$  layer, respectively;  $V_s^{\min}$  and  $V_s^{\max}$  are the minimum and maximum of the S-wave velocity, respectively;  $Thk^{\min}$  and  $Thk^{\max}$  are the minimum and maximum of the layer thickness, respectively;  $r$  is a random number uniformly distributed in the range (0, 1). We set  $V_s^{\min}$  and  $V_s^{\max}$  to 100 m/s and 700 m/s respectively, and set  $Thk^{\min}$  and  $Thk^{\max}$  to 1 m and 12 m respectively.

In PSO, a trial model is called positions ( $p$ ), and each position contains a series of variables for velocity and layer thickness. Each position has a cost value equal to its objective function (Eq. (1)). The position is iteratively updated via Eqs. (5) and (6).

$$p_i^{k+1} = p_i^k + v_i^{k+1} \quad (5)$$

$$v_i^{k+1} = \omega v_i^k + a_1 r_1 (pbest_i^k - p_i^k) + a_2 r_2 (gbest^k - p_i^k) \quad (6)$$

where  $i$  is the number of particles;  $k$  is the number of iterations;  $gbest^k$  is the previous best position of the entire swarm at the  $k^{th}$  iteration;  $pbest_i^k$  is the previous best position of the  $i^{th}$  particle at the  $k^{th}$  iteration;  $p_i^k$  and  $v_i^k$  are the position and position-increment of the  $i^{th}$  particle at the  $k^{th}$  iteration, respectively;  $\omega$  is the inertia weight;  $a_1$  and  $a_2$  denote the local and global factors, respectively;  $r_1$  and  $r_2$  represent the random numbers uniformly distributed in the range (0, 1). We set the PSO parameters as  $(\omega, a_1, a_2) = (0.729, 1.494, 1.494)$  [29] in this paper. The setting of parameters is not unique, readers may need to set them reasonably according to the corresponding physical problems, there is no magical solution that is suitable for all cases [30, 31].

## 2.2 IPSO method

The main steps of IPSO are the same as traditional PSO, the key difference is that the IPSO method improves the inversion efficiency by reducing swarm size in the later iterations, and improves the global optimal solution searching capability by replacing the invalid particles with the valid ones.

We judge two particles to be similar if their cost (equal to the objective function, Eq. (1)) and  $RMSE^V$  (the RMSE of the model's S-wave velocities) are close to each other, and the particle with the larger cost is called invalid particle. Performing similarity determination on all particles in the swarm, and the particles retained after eliminating all invalid particles are called valid particles. The particles tend to concentrate as the number of iterations increases, and invalid particles take up a large number in the later iterations. The invalid particles contribute little to the iteration, but have the same computation with the valid ones, thus need to be replaced with the newly generated valid ones. Since the particle similarity judgement is computationally huge, we need to do it after the particles have converged sufficiently, therefore, we perform one invalid particle judgement and replacement every several iterations ( $N$ ).

We record the S-wave velocity at depth intervals of 0.1 m for the strata model within a depth of 40 m, and calculate the RMSE of the S-wave velocities between the inverted and true models (Eq. (7)).

$$RMSE^V = \left( \sum_{i=1}^D (V_i^{true} - V_i^{inv})^2 / D \right)^{1/2} \quad (7)$$

where  $RMSE^V$  is the RMSE of the model's S-wave velocities;  $V_i^{true}$  and  $V_i^{inv}$  are the S-wave velocities of the true and inverted models at the  $i^{th}$  depth point, respectively;  $D$  is the number of depth points.

The main step of IPSO method for FVSI are briefly described below:

(1) Importing the initial parameters.

Importing the necessary parameters, such as early iteration number ( $K_1$ ), later iteration number ( $K_2$ ), swarm number in the early iterations ( $M_1$ ), swarm number in the later iterations ( $M_2$ ), iteration number for each particles replacement ( $N$ ), iteration termination cost ( $\Phi^T$ ), and the weighting factors ( $\omega, a_1, a_2$ ).

(2) Generating the initial particles and calculating their properties.

Randomly and automatically generating  $M_1$  initial particles within the searching space ( $V_s^{\min}, V_s^{\max}, Thk^{\min}, Thk^{\max}$ ), and calculating the corresponding properties such as position ( $p$ ), position-increment ( $v$ ), cost ( $\Phi$ ),  $gbest$  and  $pbest$ . The initial position-increments ( $v$ ) are set to zero,  $pbest$  is the particle itself,  $gbest$  is the particle with the minimal cost in the swarm.

(3) Iteratively updating the particles for  $K_1$  times.

Calculating new particles basing on the particles' properties ( $v, \Phi, pbest, gbest$ ) of the last iteration, and repeatedly updating the particles (via Eqs. (5) and (6)) for  $K_1$  times.

(4) Selecting  $M_2$  new initial particles.

Selecting  $M_2$  particles with the smaller cost as the new initial particles.

(5) Iteratively updating the particles for  $K_2$  times.

We firstly perform the particle similarity judgement, and eliminate the invalid particles. If the number of the remained valid particles is less than  $M_2$ , we will randomly generate the corresponding number of new particles (via Eqs. (3) and (4)). We then calculate the new particles' properties, and repeatedly update the particles (via Eqs. (5) and (6)) for  $K_2$  times.

In addition, during the performance of steps (3) and (5), if the cost of a particle is less than the termination cost ( $\Phi^T$ ), the iteration will be terminated prematurely. The flowchart of IPSO is shown in Figure 1, the parameters using in this study is shown in Table 1.

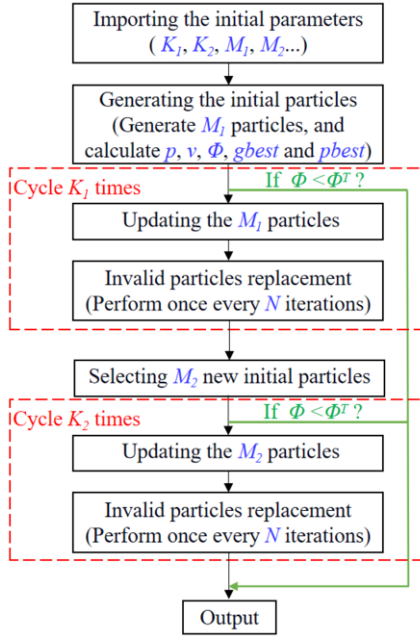


Figure 1. The flowchart of IPSO.

Table 1. Parameters of IPSO.

$K_1$	$K_2$	$M_1$	$M_2$	$N$	$\omega$	$a_1$	$a_2$
20	80	128	64	20	0.729	1.494	1.494

Table 2. Parameters of the  $M_1$  model.

Layer No.	S-wave velocity (m/s)	Thickness (m)	Poisson's ratio	Density (g/cm <sup>3</sup> )
1	300	5	0.35	2.0
2	200	10	0.35	2.0
3	300	10	0.35	2.0
4	400	$\infty$	0.35	2.0

### 3. Effectiveness analysis

We set up a theoretical model (denoted as  $M_1$  model) in Table 2, and we will use its theoretical FVS (shown in Figure 2) as the observed data for all the following synthetic examples. To reduce the influence of the source energy differences on inversion, the FVS has been normalized between 0 and 1. Since density and Poisson's ratio are less important in Rayleigh wave inversion, we set them to fixed values. We perform the FVSI via PSO method with the same weighting factors ( $\omega, a_1, a_2$ ) as the IPSO method (shown in Table 1). We set the other parameters in PSO inversion with the number of the maximum iterations of 100 ( $K$ ), and the number of particles in the swarm of 128 ( $M$ ).

We judge two particles are similar if the absolute value of the cost difference ( $\Phi^R$ ) is less than 0.02, and the absolute value of the  $RMSE^V$  difference ( $RMSE^{V-R}$ ) is less than 10 m/s. The similar particles take up a lot of computational resources but have little effect

on the inversion results. We show two groups of particles with similarities in Table 3 and Figure 3.

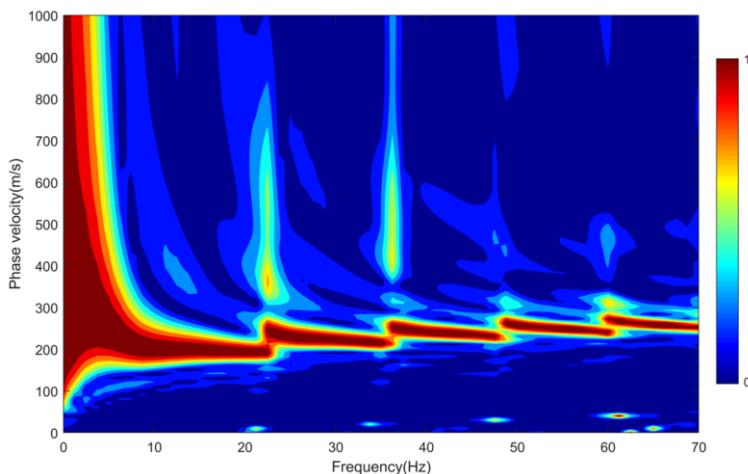


Figure 2. The FVS of  $M_1$  model.

Table 3. Parameters of the similar particles (corresponding models).

Model	$Vs^1$	$Vs^2$	$Vs^3$	$Vs^4$	$Thk^1$	$Thk^2$	$Thk^3$	$\Phi$	$\Phi^R$	$RMSE^{V-R}$
T <sub>1</sub>	172	219	359	554	5.1	3.0	3.2	0.1506	0.0017	7.6
T <sub>2</sub>	169	223	360	552	5.2	3.0	3.1	0.1523		
T <sub>3</sub>	170	218	351	572	5.4	2.9	3.3	0.1482	0.0145	7.5
T <sub>4</sub>	167	213	358	573	5.4	2.8	3.4	0.1627		

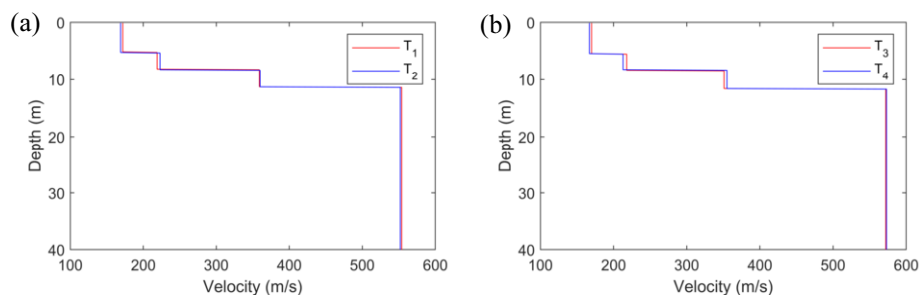
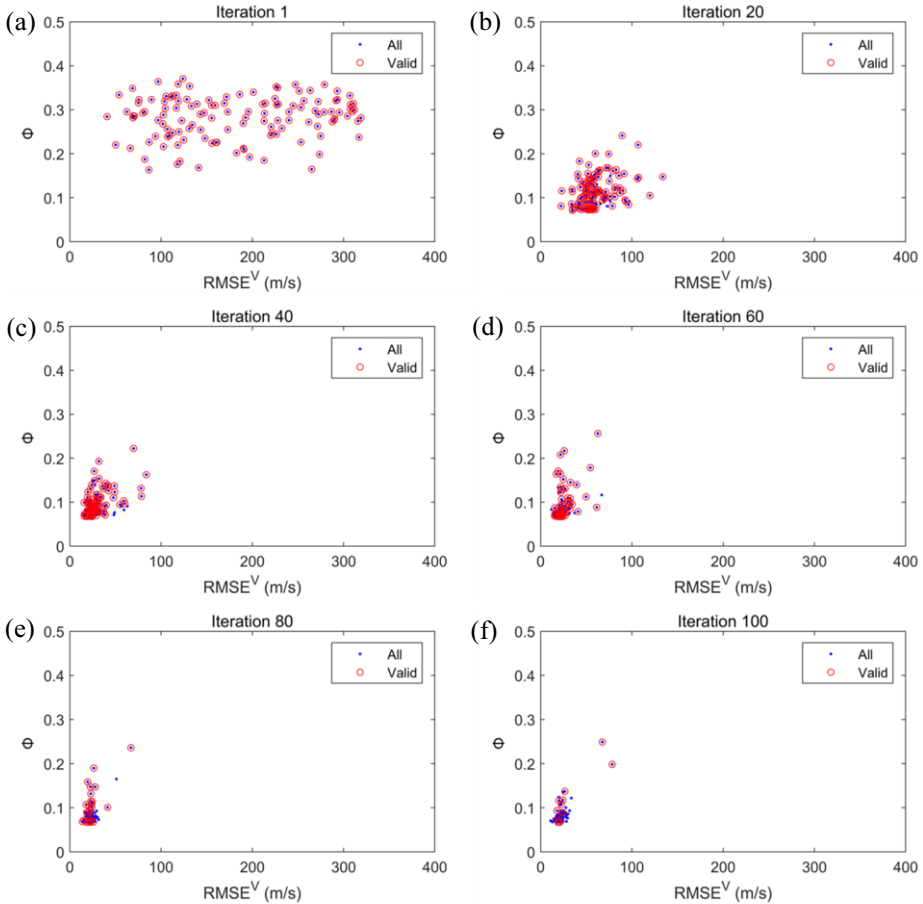


Figure 3. The comparisons of the similar particles (corresponding models).

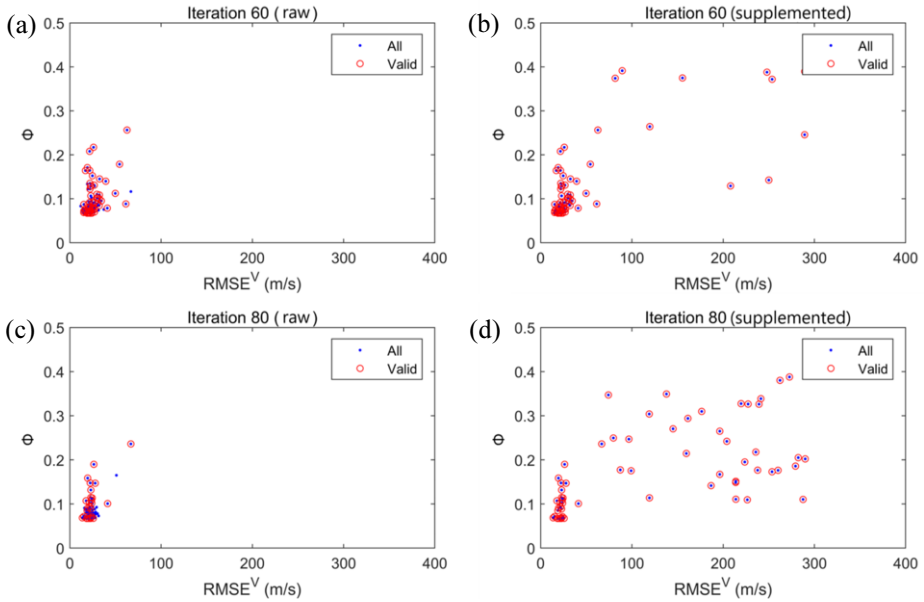
In Table 3, the  $Vs^i$  and  $Thk^i$  are the S-wave velocity and thickness of the  $i^{th}$  layer respectively ( $i = 1, 2, 3, 4$ );  $\Phi$  is the cost equal to the RMSE of FVS;  $\Phi^R$  is the absolute value of the cost difference;  $RMSE^{V-R}$  is the absolute value of the  $RMSE^V$  difference. We can see that the cost of T<sub>2</sub> ( $\Phi = 0.1523$ ) is larger than that of T<sub>1</sub> ( $\Phi = 0.1506$ ), so the particle corresponding to T<sub>1</sub> model is called valid particle, and the particle corresponding to T<sub>2</sub> model is called invalid particle. Similarly, the particle corresponding to T<sub>3</sub> model is called valid particle, and the particle corresponding to T<sub>4</sub> model is called invalid particle.

The invalid particles will be eliminated, and the particles that remain after eliminating all the invalid particles are called valid particles. We respectively regard the cost and  $RMSE^V$  as the horizontal and vertical coordinates, and the particles spatial distribution during PSO inversion is shown in Figure 4. It is obvious that as the iterations increase, the particles tend to concentrate and the valid particles gradually decrease. In other words, there is a large number of invalid computations performed in the later iterations in traditional PSO inversion. Therefore, it is reasonable and efficient that we eliminate the invalid particles and supplement them with randomly generated valid particles.



**Figure 4.** The particles spatial distribution that changes with iteration. (a), (b), (c), (d), (e) and (f) denote the particle distributions of the 1<sup>st</sup>, 20<sup>th</sup>, 40<sup>th</sup>, 60<sup>th</sup>, 80<sup>th</sup> and 100<sup>th</sup> iterations. The blue points represent all the particles of the swarm, which are 128 in each iteration. The red circles represent the valid particles, which are 128, 88, 61, 42, 26 and 14, respectively.

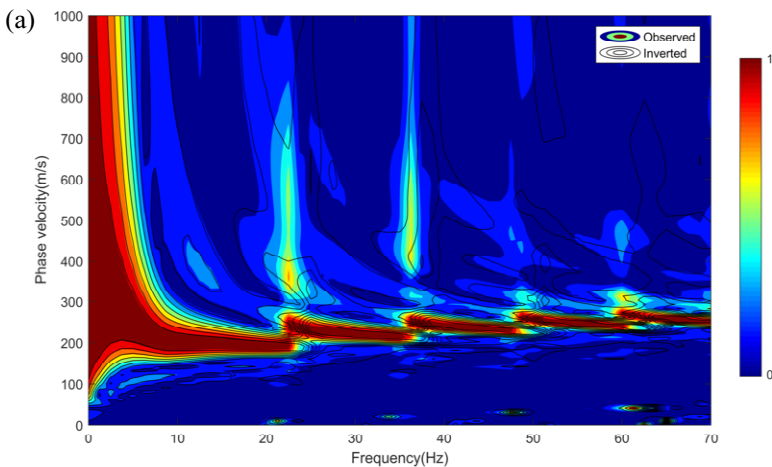
We take the 60<sup>th</sup> and 80<sup>th</sup> iterations in Figure 4 as an example to show the effect of supplementing the randomly generated valid particles, and their results are shown in Figure 5. We see that the particles supplementation increases the valid particles significantly, which improves the capability of the algorithm to search for globally optimal solutions.



**Figure 5.** The particles spatial distribution before and after particles supplementation. (a) and (c) represent the particle distributions of the 60<sup>th</sup> and 80<sup>th</sup> iterations before particles supplementation. (b) and (d) represent the particle distributions of the 60<sup>th</sup> and 80<sup>th</sup> iterations after particles supplementation. The blue points represent all the particles of the swarm, which are 128 in each iteration. The red circles represent the valid particles, which are 42, 64, 26 and 64, respectively.

### 4. Synthetic example

We perform a comparison between PSO and IPSO inversions to verify the superiority of the IPSO method. We use the theoretical FVS (Figure 2) as the observed data, and then perform the FVSI via PSO and IPSO methods respectively. The PSO and IPSO inverted FVS are shown in Figure 6 and Figure 7, respectively; the model parameters are shown in Table 4; the model and iterative error curve comparisons are shown in Figure 8.



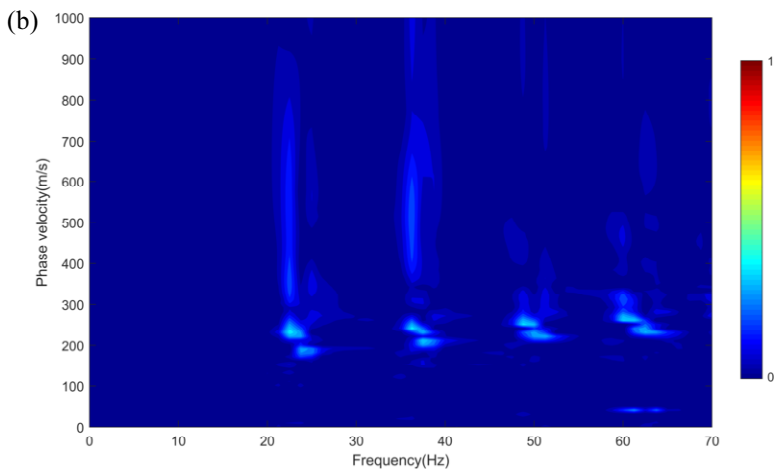


Figure 6. The FVS of PSO inversion in synthetic data. (a) is the comparison of observed and inverted FVS, where the background colors and overlapped contour lines represent the observed and inverted FVS, respectively. (b) is the absolute of the FVS residuals.

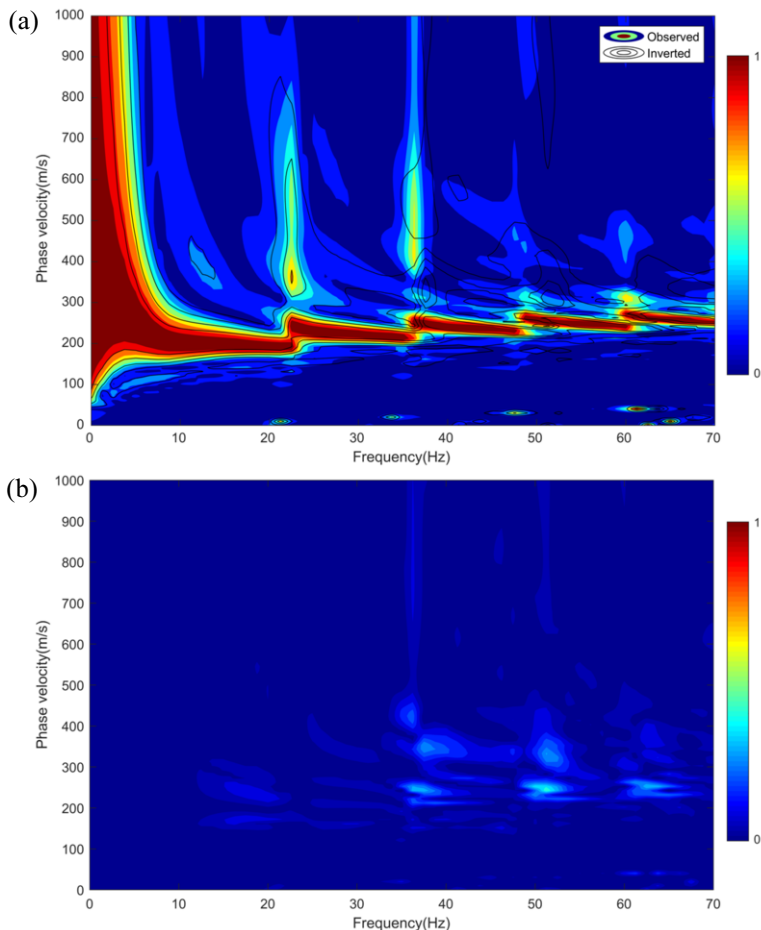
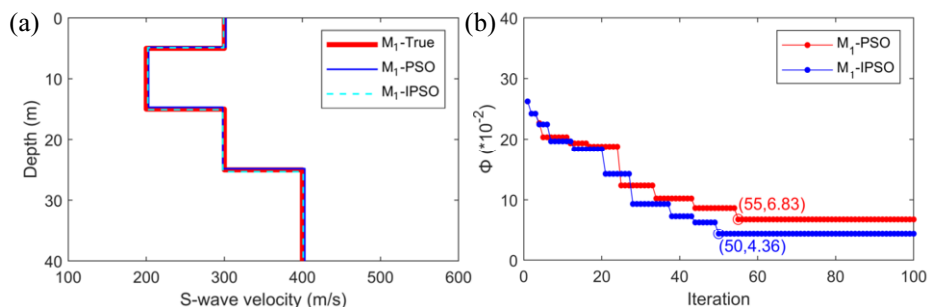


Figure 7. The FVS of IPSO inversion in synthetic data. (a) is the comparison of observed and inverted FVS, where the background colors and overlapped contour lines represent the observed and inverted FVS, respectively. (b) is the absolute of the FVS residuals.



**Figure 8.** The model and iterative error curve comparisons for PSO and IPSO in synthetic data inversions. (a) is the model comparison, where  $M_1$ -True represents the true model,  $M_1$ -PSO represents the PSO inverted model, and  $M_1$ -IPSO represents the IPSO inverted model. (b) is the iterative error curves comparison, where  $M_1$ -PSO represents the PSO inverted result, and  $M_1$ -IPSO represents the IPSO inverted result.

**Table 4.** The comparison of model parameters in synthetic data inversion.

Model	$V_s^1$	$V_s^2$	$V_s^3$	$V_s^4$	$Thk^1$	$Thk^2$	$Thk^3$	$\Phi$	$RMSE^V$
<b>M<sub>1</sub>-True</b>	300	200	300	400	5	10	10	0	0
<b>M<sub>1</sub>-PSO</b>	302	203	298	403	4.8	9.9	10.1	0.0683	13.4
<b>M<sub>1</sub>-IPSO</b>	299	202	298	401	4.9	10.2	10.2	0.0436	11.3

In Table 4, the RMSE of the spectrum for IPSO inversion ( $\Phi = 0.0436$ ) is less than that of PSO inversion ( $\Phi = 0.0683$ ), and the RMSE of the models' S-wave velocities for IPSO inversion ( $RMSE^V = 11.3$ ) is also less than that of PSO inversion ( $RMSE^V = 13.4$ ), which indicates that the inversion result of IPSO is more accurate than that of PSO. In Figure 8, the PSO inversion converges at the 55<sup>th</sup> iteration, and the IPSO inversion converges at the 50<sup>th</sup> iteration, which means the IPSO method is more efficient than the PSO method.

In addition, for the PSO inversion, the number of particles is 128 ( $M$ ), the number of iterations is 100 ( $K$ ), and the total number of forward modeling is 12928 ( $= 128 + 128 * 100$ ). In contrast, for the IPSO inversion (adopting the parameters in Table 1), the number of particles is 128 ( $M_1 = 128$ ) for the early iterations ( $K_1 = 20$ ), and reduces to 64 ( $M_2 = 64$ ) for the later iterations ( $K_2 = 80$ ), thus, the total number of forward modeling is 7808 ( $= 128 + 128 * 20 + 64 * 80$ ). Compared to traditional PSO, IPSO method is less computational and more efficient.

### 5. Field data application

In order to further test the effectiveness of the IPSO method for field data application, we acquire the seismic data from Wuhan, Hubei Province, China, over a wide area of undisturbed stratigraphy. We collect the seismic records by a 24-channel seismograph with 4.5 Hz vertical geophones, and using an 18-pound hammer as the seismic source. The geophones are arranged at equal intervals with a spacing of 1 m, and the minimum distance between the geophones and the source is 4 m. Each channel has 2048 sampling points with a sampling interval of 0.2 ms.

According to the available borehole data, the stratigraphy of the survey area is roughly divided into three layers, i.e., the 1<sup>st</sup> layer of loose clay (depth from 0 to 7.1 m), the 2<sup>nd</sup> layer of coarse sand (depth from 7.1 to 12.2 m), and the 3<sup>rd</sup> layer of sandstone (depth greater than 12.2 m). To improve the inversion difficulty, we set the inversion model to 4 layers and test the effect of the IPSO method when the number of inversion layers is unknown. The field seismic records and corresponding FVS are shown in Figure 9. We respectively perform the FVSI via PSO and IPSO methods, the FVS comparisons are shown in Figure 10 and Figure 11, the corresponding model comparisons are shown in Figure 12, and the model parameter statistics is shown in Table 5. We see that the PSO and IPSO inverted FVS match well with the measured FVS (Figure 10 and Figure 11), and the inverted models also agree well with the borehole (Figure 12), which suggests that the IPSO method is accurate and reliable.

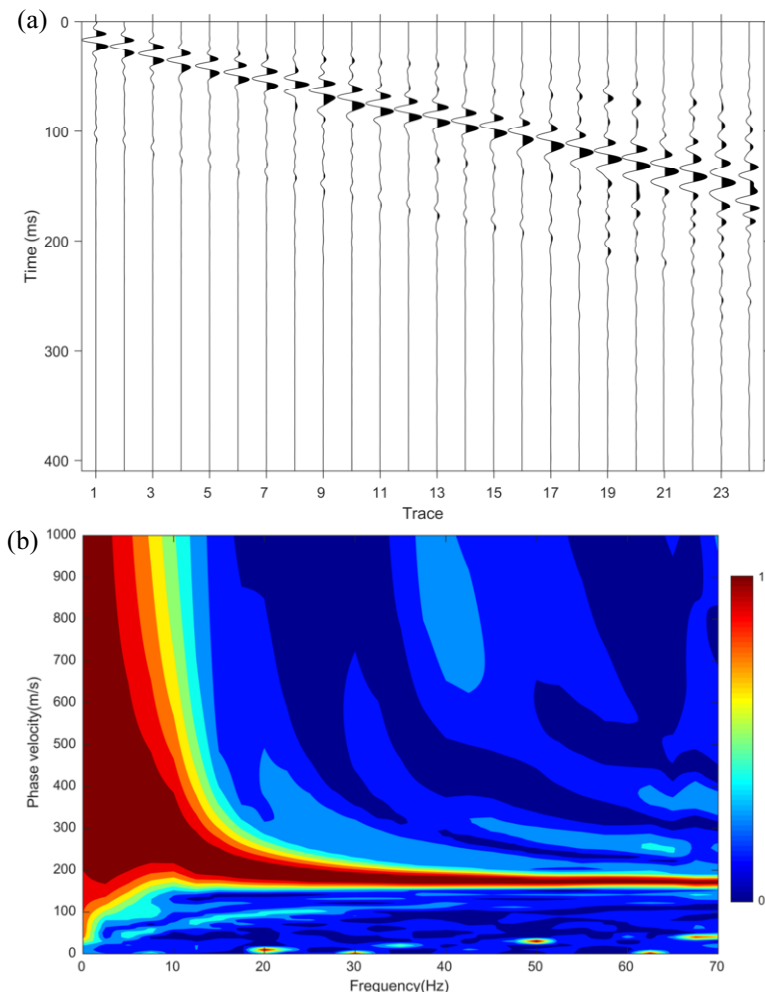


**Figure 9.** The waveform and FVS of the field data. (a) is the waveform. (b) is the corresponding FVS.

In addition, the first layer of the real stratigraphy is divided into two layers with similar velocities in the inverted model, which shows that the IPSO method still performs well when the number of inversion layers is unknown. As shown in Figure 12(b) and Table 5, the PSO inversion converges at the 60<sup>th</sup> iteration with a minimum misfit value of 16.56, while the IPSO inversion converges at the 52<sup>th</sup> iteration with a minimum misfit value of 13.65, which suggests the IPSO method is more accurate and efficient than the PSO method.

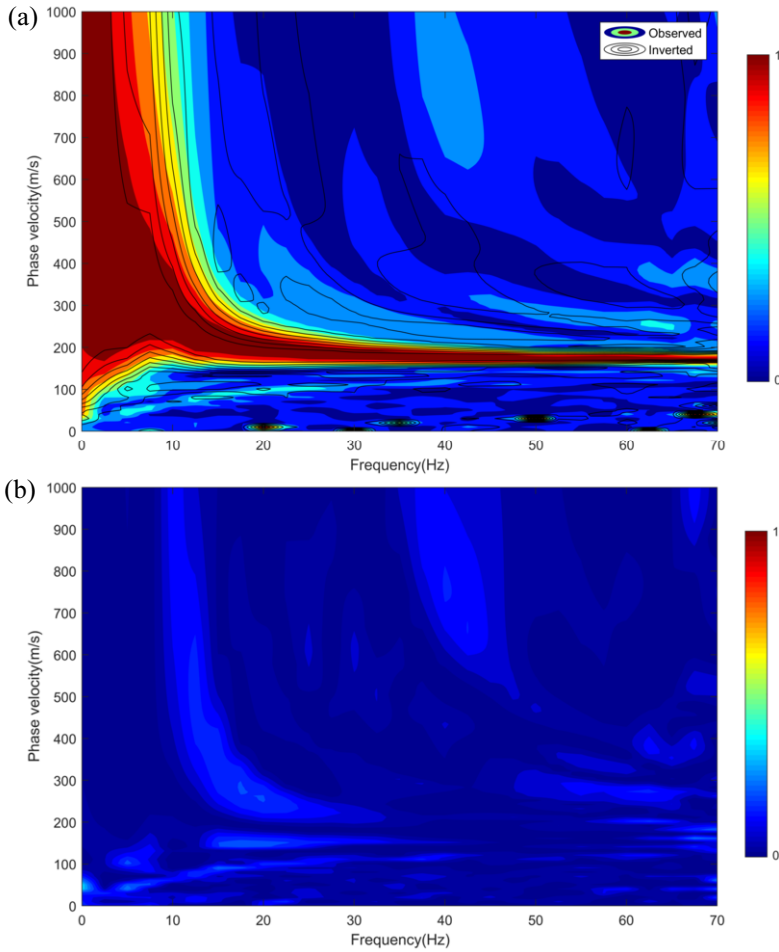


**Figure 10.** The FVS of PSO inversion in field data. (a) is the comparison of observed and inverted FVS, where the background colors and overlapped contour lines represent the observed and inverted FVS, respectively. (b) is the absolute of the FVS residuals.

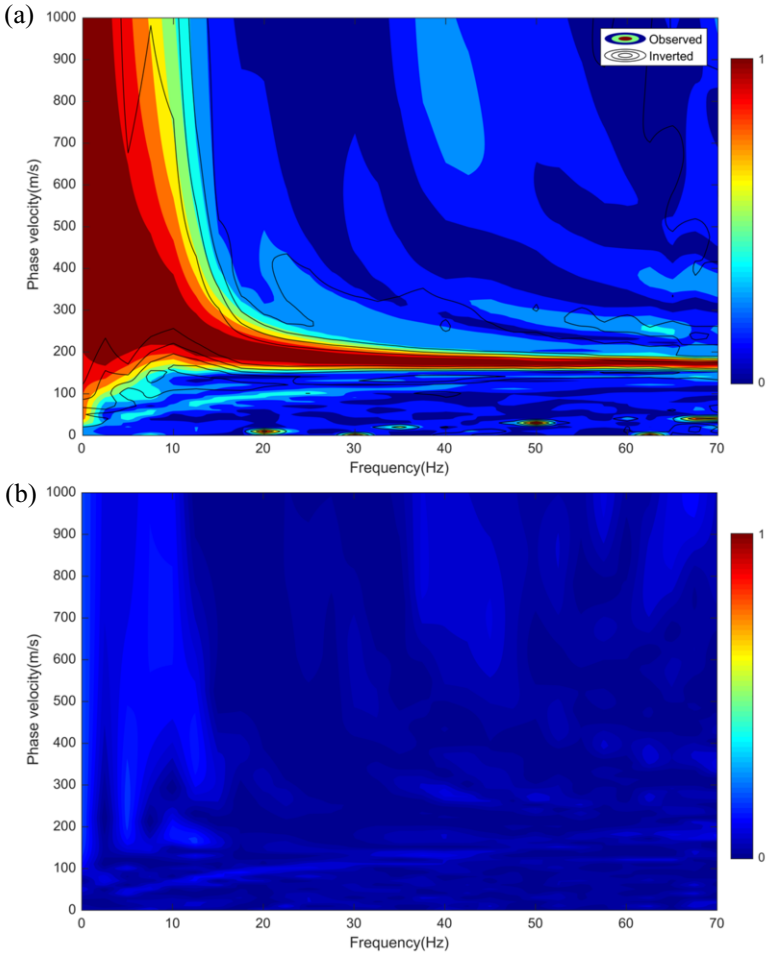


**Figure 11.** The FVS of IPSO inversion in field data. (a) is the comparison of observed and inverted FVS, where the background colors and overlapped contour lines represent the observed and inverted FVS, respectively. (b) is the absolute of the FVS residuals.

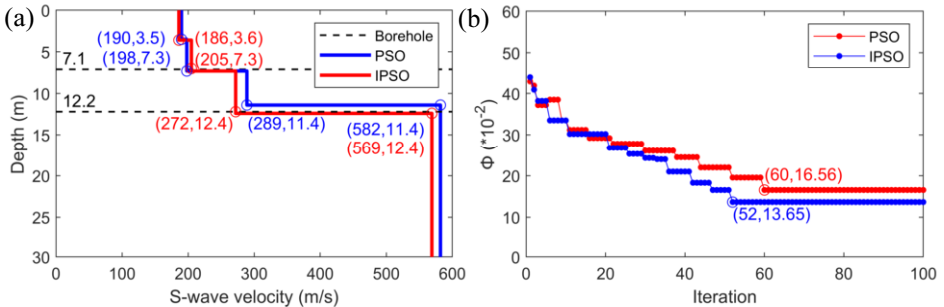


**Figure 12.** The model and iterative error curve comparisons for PSO and IPSO in field data inversions. (a) is the model comparison, where the black dashed lines and texts represent the borehole, the blue lines and texts represent the PSO inverted model, and the red lines and texts represent the IPSO inverted model. (b) is the iterative error curves comparison, where the red dots and lines represent the PSO inverted result, and the blue dots and lines represent the IPSO inverted result.

**Table 5. The comparison of model parameters in field data inversion.**

Model	$V_s^1$	$V_s^2$	$V_s^3$	$V_s^4$	$Thk^1$	$Thk^2$	$Thk^3$	$\Phi$
Borehole	—	—	—	—	—	7.3	5.1	—
PSO	190	198	289	582	3.5	3.8	4.1	0.1656
IPSO	186	205	272	569	3.6	3.7	5.1	0.1365

## 6. Conclusions

We propose an IPSO method for Rayleigh wave FVSI, and achieve good results in both synthetic and field examples. Compared with traditional PSO, the IPSO has a large swarm size in the early iterations, and a smaller swarm size in the later iterations. A large swarm size helps to improve the capability of searching for globally optimal solutions, and a smaller swarm size helps to make the inversion more efficient. We introduce a criterion for judging similar particles in FVSI, and the similar particles have equal amounts of computation but have little effect on the inversion results. We enhance the ability of searching for global solutions by eliminating invalid particles and randomly generating valid particles, which makes the inversion results more accurate. The good results from synthetic and field examples indicate that the IPSO is an effective and practicable method for Rayleigh wave FVSI, and the application in this paper is just one of the scenarios of the method, and we look forward to more people using the IPSO method in more areas.

## Acknowledgements

This study is funded by the National Natural Science Foundation of China (No. 41674142).

## References

- [1] Xia, J., Miller, R.D., Park, C.B. Estimation of near-surface shear-wave velocity by inversion of Rayleigh wave. *Geophysics*. 1999; 64: 691–700.
- [2] Xia, J. Estimation of near-surface shear-wave velocities and quality factors using multichannel analysis of surface-wave methods. *Journal of Applied Geophysics*. 2014; 103: 140–151.
- [3] Zhang, S.X. Effective dispersion curve and pseudo multimode dispersion curves for Rayleigh wave. *Journal of Earth Science*. 2011; 22: 226–230.
- [4] Knopoff, L. A matrix method for elastic wave problems. *Bulletin of the Seismological Society of America*. 1964; 54: 431–438.
- [5] Chen, X. A systematic and efficient method of computing normal modes for multi-layer half-space. *Geophysical Journal International*. 1993; 115: 391–409.
- [6] Wang, J., Wu, G., Chen, X. Frequency-Bessel transform method for effective imaging of higher-mode Rayleigh dispersion curves from ambient seismic noise data. *Journal of Geophysical Research: Solid Earth*. 2019; 124: 3708–3723.
- [7] Tarantola, A. Inversion of seismic reflection data in the acoustic approximation. *Geophysics*. 1984; 49: 1259–1266.
- [8] Groos, L., Schäfer, M., Forbriger, T., et al. Application of a complete workflow for 2D elastic full-waveform inversion to recorded shallow-seismic Rayleigh waves. *Geophysics*. 2017; 82: R109–R117.

- [9] Pan, Y., Gao, L., Bohlen, T. Time-domain full-waveform inversion of Rayleigh and love waves in presence of free-surface topography. *Journal of Applied Geophysics*. 2018; 152: 77–85.
- [10] Yan, Y., Wang, Z., Li, J., Huai, N., et al. Elastic SH- and Love-wave Full-Waveform Inversion for shallow shear wave velocity with a preconditioned technique. *Journal of Applied Geophysics*. 2020; 173: 103947.
- [11] Le, Z., Song, X., Zhang, X., et al. Multi-objective particle swarm optimization for Rayleigh wave full waveform inversion. *Journal of Applied Geophysics*. 2023; 215: 105096.
- [12] Yuan, Y.O., Simons, F.J., Bozdağ, E. Multiscale adjoint waveform tomography for surface and body waves. *Geophysics*. 2015; 80 (5): R281–R302.
- [13] Gao, L., Pan, Y. Source signature estimation from multimode surface waves via mode-separated virtual real source method. *Geophysical Journal International*. 2018; 213: 1177–1186.
- [14] Wang, T., Guan, J., Yang, Z., et al. Utility tunnel detection by 2D elastic PSV/Rayleigh-wave multi-parameter full waveform inversion. *Journal of Applied Geophysics*. 2023; 214: 105087.
- [15] Solano, C.P., Donno, D., Chauris, H. 2D surface wave inversion in the F-K domain. In 75th EAGE Conference and Exhibition incorporating SPE EUROPEC. 2013.
- [16] Pérez Solano, C., Donno, D., Chauris, H. Alternative waveform inversion for surface wave analysis in 2-D media. *Geophysical Journal International*. 2014; 198(3): 1359–1372.
- [17] Dal Moro, G., Moura, R.M.M., Moustafa, S. Multi-component joint analysis of surface waves. *Journal of Applied Geophysics*. 2015; 119: 128–138.
- [18] Zhang, Z., Saygin, E., He, L., et al. Rayleigh Wave Dispersion Spectrum Inversion Across Scales. *Surveys in Geophysics*. 2021; 42: 1281–1303.
- [19] Park, C.B., Miller, R.D., Xia, J. Imaging dispersion curves of surface waves on multi-channel record. SEG Technical Program Expanded Abstracts. 1998; 1377–1380.
- [20] Foti, S., Hollender, F., Garofalo, F., et al. Guidelines for the good practice of surface wave analysis: a product of the Inter PACIFIC project. *Bulletin of Earthquake Engineering*. 2018; 16 (6): 2367–2420.
- [21] Li, J., Hanafy, M.S. Skeletonized inversion of surface wave: active source versus controlled noise comparison. *Interpretation*. 2016; 3: 11–19.
- [22] Li, J., Feng, Z., Schuster, G. Wave-equation dispersion inversion. *Geophysical Journal International*. 2017; 208 (3): 1567–1578.
- [23] Zhang, Z., Schuster, G.T., Liu, Y., et al. Wave equation dispersion inversion using a difference approximation to the dispersion-curve misfit gradient. *Journal of Applied Geophysics*. 2016; 133: 9–15.
- [24] Kennedy, J., Eberhart, R.C. Particle Swarm Optimization. *Proceedings of the IEEE International Conference on Neural Networks*. 1995; 4: 1942–1948.
- [25] Shi, Y., Eberhart, R.C. Parameter selection in particle swarm optimization. *Evolutionary Programming*. 1998; VII: 591–600.
- [26] Le, Z., Song, X., Zhang, X., et al. Particle swarm optimization for Rayleigh wave frequency-velocity spectrum inversion. *Journal of Applied Geophysics*. 2024; 222: 105311.
- [27] Virieux, J. P-SV wave propagation in heterogeneous media: velocity-stress finite-difference method. *Geophysics*. 1986; 51 (4): 889–901.
- [28] Bohlen, T. Parallel 3-D viscoelastic finite-difference seismic modeling. *Computers & Geosciences*. 2002; 28: 887–899.
- [29] Clerc, M.A., Kennedy, J. The particle swarm-explosion, stability, and convergence in a multidimensional complex space. *IEEE Transactions on Evolutionary Computation*. 2002; 6 (1): 58–73.
- [30] Fernández Martínez, J.L., García Gonzalo, E., Fernández Álvarez, J.P., et al. PSO: a powerful algorithm to solve geophysical inverse problems: application to a 1D-DC resistivity case. *Journal of Applied Geophysics*. 2010; 71: 13–25.
- [31] Ai, H., Essa, K.S., Ekinici, Y.L., et al. Magnetic anomaly inversion through the novel barnacles mating optimization algorithm. *Scientific Reports*. 2022; 12: 22578.